Investigation of Clusters in Medium Carbon Secondary Hardening Ultra-high-strength Steel After Hardening and Aging Treatments

R. VEERABABU, R. BALAMURALIKRISHNAN, K. MURALEEDHARAN, and M. SRINIVAS

Clusters, containing between 10 and 1000 atoms, have been investigated in a martensitic secondary hardening ultra-high-strength steel austenitized at 1173 K (900 °C) for 1 hour and tempered at either 768 K or 783 K (495 °C or 510 °C) for 4 or 8 hours using 3D atom probe. The presence of clusters was unambiguously established by comparing the observed spatial distribution of the different alloying elements against the corresponding distribution expected for a random solid solution. Maximum separation envelope method has been used for delineating the clusters from the surrounding "matrix." Statistical analysis was used extensively for size and composition analyses of the clusters. The clusters were found to constitute a significant fraction accounting for between 1.14 and 2.53 vol pct of the microstructure. On the average, the clusters in the 783 K (510 °C) tempered sample were coarser by ~65 pct, with an average diameter of 2.26 nm, relative to the other samples. In all samples, about 85 to 90 pct of the clusters have size less than 2 nm. The percentage frequency histograms for carbon content of the clusters in 768 K and 783 K (495 °C and 510 °C) tempered samples revealed that the distribution shifts toward higher carbon content when the tempering temperature is higher. It is likely that the presence of these clusters exerts considerable influence on the strength and fracture toughness of the steel.

DOI: 10.1007/s11661-015-2843-2
© The Minerals, Metals & Materials Society and ASM International 2015

I. INTRODUCTION

SECONDARY hardening ultra-high-strength (SHUHS) steels, containing significant amounts of cobalt and nickel, possess excellent combination of strength, fracture toughness (K_{IC}), and stress corrosion cracking resistance (K_{ISCC}). These steels have been used for niche applications such as aircraft landing gear, armor, *etc.*, due to their unique combination of properties. Some typical steels of this type are HY180, AF1410, and AerMet100.[1-4] These are essentially quenched and tempered steels that derive their strength and toughness from fine M_2C carbides present in a highly dislocated lath martensitic structure.[5] The optimum heat treatment for these steels, corresponding to a slightly overaged condition, consists of austenitizing in the range 1098 K to 1173 K (825 °C to 900 °C), followed by quenching to room temperature and LN_2 treatment and tempering in the range 758 K to 783 K(485 °C to 510 °C) for 5 hours.[1,6]

The microstructure of these steels in the as-quenched condition consists essentially of lath martensite. Depending on the austenitizing temperature, small amounts of undissolved primary carbides such as MC, M_6C, and $M_{23}C_6$ may also be present.[3,6] The typical tempering behavior of these steels has been extensively described in the literature[1,3,7-11]: at lower tempering temperatures [~698 K (~425 °C)], coarse cementite is formed, which is associated with a drop in toughness. At higher tempering temperatures [723 to 773 K (450 to 500 °C)], needle-shaped coherent M_2C precipitates are formed along ⟨100⟩ direction of ferrite. Even though M_6C and $M_{23}C_6$ are thermodynamically more stable carbides than M_2C, the higher coherency of M_2C with the matrix has been reported to be responsible for its precipitation prior to that of the other carbides.[6] At even higher temperatures, the needle-shaped M_2C precipitates begin to coarsen resulting in a slight loss of strength but accompanied by a disproportionate increase in toughness. For this reason, all secondary hardening steels are put into service in this slightly overaged condition. It has been reported that the observation and confirmation of M_2C in this optimally heat-treated condition is often difficult due to small size of the precipitates (in spite of slight coarsening) and the high dislocation density of lath martensitic microstructure. However, Ayer *et al.*,[3] Stiller *et al.*,[12] and Akre *et al.*,[13] using TEM of extraction replicas, field-ion microscopy, and 3D atom probe, respectively, have been able to show that at least some of the precipitates are of M_2C type.

In addition to M_2C strengthening carbide, several fine clusters were reported recently in the SHUHS steel using 3D atom probe investigations.[14] It has been reported

R. VEERABABU, R. BALAMURALIKRISHNAN, and M. SRINIVAS, Scientists, are with the Defence Metallurgical Research Laboratory, Hyderabad 500058, India. Contact e-mail: veeruiisc@gmail.com K. MURALEEDHARAN, Scientist, Director Technical (Materials), is with the Technical Core Group, DRDO Head Quarters, New Delhi 110 011, India.

Manuscript submitted January 24, 2014.
Article published online March 18, 2015

that clusters exert a significant influence on the mechanical properties. For example, Xie *et al.*[15] have reported that Nb-rich clusters can contribute to yield strength increments of the order of 165MPa in an Nb micro-alloyed steel. Cluster, here, refers to an aggregate of small number of solute atoms without a specific crystal structure, while precipitate contains a definite crystal structure with a relatively higher number of solute atoms.[16] The clusters are often perceived as transient/metastable forms of equilibrium precipitates. It has been reported[17] that they form more easily than the equilibrium precipitates since the misfit strain energy contribution to the free energy of formation is negligible. While there is broad general agreement on the above distinction between a cluster and a precipitate, the definition of cluster size is quite arbitrary. Solute aggregates with 2 to 10 atoms[18] as well as >1000 atoms[19] have been considered as clusters. However, some indications regarding the size of a cluster may be derived based on the specific alloy system. For example, in work on 2024 Al alloy, Sha *et al.*[20] have treated solute aggregates with 10-100 atoms as clusters, 100-1000 atoms as GPB (Guinier–Preston–Bagaryatsky) zones, and >1000 atoms as S-phase precipitates. The composition, size, and number density of the clusters evolve continuously during the aging process. In general, for a given aging/tempering temperature conducive for over aging, the number density decreases with increasing aging time and eventually becomes zero at a particular instance of time since all the clusters get converted to equilibrium precipitates.[20] Clusters can influence the formation of equilibrium precipitates in at least two ways: (a) by acting as potential nucleation sites in addition to dislocations, grain boundaries, *etc.*, and (b) by agglomeration of small clusters accompanied by atomic rearrangements.

Recently, the characterization of solute clusters by atom probe technique has received considerable attention. The relevant body of literature spans many important alloy systems such as Al alloys,[20,21] Mg alloys,[22] Cu alloys,[23] micro-alloyed steels,[15,17,18] and maraging steels.[19,24] However, the studies of clusters in secondary hardening ultra-high-strength steels appear to be rather limited.[25] We had earlier reported[14] the presence of clusters in an experimental secondary hardening ultra-high-strength steel, with composition as given in Table I. The samples had been austenitized at 1173 K (900 °C) for 1 hour, followed by oil quenching, subjected to refrigeration in LN_2 for 2 hours, and subsequently tempered at 758 K (485 °C) for 4 and 8 hours. Atom probe studies showed that the clusters appear to have a wide range of composition. In particular, it was observed that the carbon content was varying from 0 to 40 apct. The objective of the present work is to investigate the clusters in the experimental SHUHS steel austenitized at 1173 K (900 °C) for 1 hour and aged at 768 K (495 °C) for 4 or 8 hours and 783 K (510 °C) for 8 hours using 3D atom probe. The question arises as to whether these clusters are also present in optimally aged (tempered at 768 K (495 °C) for 4 or 8 hours) and overaged (tempered at 783 K (510 °C) for 8 hours) microstructures. Optimally aged is taken to represent that condition in which maximum toughness is observed with only a slight loss of strengthening as compared to peak strength. Overaged represents a condition where there is a significant loss of strength and also some loss of toughness. The present work therefore focuses on clusters present in the experimental secondary hardening ultra-high-strength steel, after tempering for either 4 or 8 hours at 768 K (495 °C) (optimally aged) and after tempering for 8 hours at 783 K (510 °C) (overaged). For the sake of comparison and detailed analysis, 3D atom probe results from the samples tempered at 758 K (485 °C) are also included here.

Table I. Composition (in Weight Percent) of the Experimental UHS Steel[14]

C	Co	Ni	Cr	Mo	V	Fe
0.37	14.8	13.7	2.0	1.0	0.2	bal

II. EXPERIMENTAL METHODOLOGY

The steel under investigation was produced in a 40-kg batch by vacuum induction melting of electrolytically pure raw materials and pouring, under vacuum, into a rectangular mold of 100 × 300 mm cross section. The resultant ingot was homogenized at 1323 K (1050 °C) for 24 hours and subsequently radiographed, and the defective "pipe" portions were removed. The sound portion of the ingot was soaked at 1323 K (1050 °C) for 4 hours and hot-rolled into 15-mm-thick plates. Samples for heat treatment were cut from the rolled plate, austenitized at 1173 K (900 °C) for 1 hour, oil quenched to room temperature, and subsequently LN_2 treated to minimize retained austenite. The samples were then subjected to tempering at different temperatures, *viz.*, 758 K, 768 K, and 783 K (485 °C, 495 °C, and 510 °C) for either 4 or 8 hours, followed by quenching in oil. Room-temperature tensile properties and fracture toughness were determined on samples machined from the heat-treated blanks, following standard ASTM testing procedures.

Thin foils for TEM examination were prepared from material obtained from the grip region of the tensile-tested samples: ~200-μm-thick slices were cut using a slow-speed saw, mechanically ground to ~100 μm thickness, and subsequently twin-jet electropolished with mixed acids (by volume: 78 pct methanol, 10 pct lactic acid, 7 pct sulfuric acid, 3 pct nitric acid, and 2 pct hydrofluoric acid) electrolyte at 243 K (−30 °C). The thin foils were examined in an FEI Tecnai 20T transmission electron microscope operated at 200 kV and equipped with an EDAX EDS system.

The atom probe specimens were prepared by the standard two-stage electropolishing method.[26] Initially, 15 to 20-mm-long blanks with 0.3 to 0.5 mm diameter were cut from tensile-tested samples using wire EDM. In the first stage, samples were polished in a solution of 25 pct perchloric acid in glacial acetic acid at 5 to 20 V DC. In the second stage, initially the samples were thinned in 6 pct perchloric acid in 2-butoxy ethanol at 5

to 20 V DC, and the final tip was formed by pulse micropolishing using 2 pct perchloric acid in 2-butoxy ethanol at 5 to 20 V DC.

Atom probe experiments were carried out on a 3D atom probe instrument originally manufactured by Oxford nano Science Ltd., Milton Keynes, The UK. Field-ion imaging was carried out at a specimen temperature of 70 K (−203 °C) with neon as the imaging gas at ~2.5×10^{-5} mbar pressure. Once a clean field-ion image was obtained, the region of interest was chosen and positioned for atom probe data acquisition which was performed at a specimen temperature of 70 K (−203 °C) and at pressures below 8×10^{-10} mbar using a 20 pct pulse fraction. Data reconstruction, visualization, and analysis were performed using the PoSAP software supplied with the instrument.

The presence of clusters/precipitates was established by comparing the solute elements distribution in the solid solution with their corresponding binomial distributions. Quantitative or semi-quantitative analysis of the clusters can be performed once they are delineated from the neighboring matrix. Several cluster finding algorithms are available such as core-linkage algorithm,[18,27] contingency table analysis,[19,23,24] maximum separation envelope method (MSEM),[26,28-30] *etc*. The latter has found wide use in cluster identification in steels and other alloys and has been adopted in this work. MSEM is based on the fact that the solute atoms in the particle are more closely spaced than in the matrix. Therefore, a solute atom within a certain distance (maximum separation distance, d_{max}) of another solute atom of the same type or group of types is considered as belonging to the particle. Other important parameters of MSEM, in addition to d_{max}, are solute elements (*e.g.*, C, Cr, and Mo for carbides) in clusters, minimum number of atoms that constitute the cluster (N_{min}), surround distance, and erosion distance. *Surround distance* is the distance around the particle in which the surrounding non-precipitate atoms (matrix atoms) are added to the particle. This parameter helps in adding matrix atoms to the particle, which actually belong to the particle. *Erosion distance* is the distance below which a particle atom closer to any matrix atom after all the surrounding atoms have been added to the particles is removed from the particle. This parameter helps in removing particle atoms that are actually belonging to the matrix. The selection of these parameters (d_{max}, N_{min}, surround distance, and erosion distance) for MSEM and core-linkage algorithms is a critical step as it affects the quantitative analysis of the identified clusters. However, there is no universally accepted methodology for parameter selection,[27] and different researchers have used varying guidelines to identify the parameters. In the present work, several values for these parameters were tested and evaluated against information available in the literature.[17,21,23,28,31-33] Through this exercise, the following parameters were found to be most optimal for performing cluster analyses: $N_{min} = 10$; $d_{max} = 0.4$ nm, surround distance = 0.2 nm, and erosion distance = 0.2 nm. The carbide-forming elements, Cr, Mo, and V, as well as carbon have been treated as the solute elements. The equivalent spherical radius, r, of a cluster has been evaluated using $r = (3n\Omega/4\pi\zeta)^{1/3}$,[26] where n is the number of ions in the cluster, Ω the atomic volume ($= 1.178 \times 10^{-2}$ nm^3 for bcc Fe), and ζ, the overall detection and reconstruction efficiency (taken to be 0.5). It should be noted that N_{min} of 10 atoms corresponds to a diameter of 0.8 nm. The composition of the clusters was calculated in atom percent, by considering the ratio of number of atoms of each individual element to the total number of atoms in the cluster/precipitate.

III. RESULTS AND DISCUSSION

A. *Mechanical Properties*

The mechanical property data for the experimental UHS steel as a function of tempering temperature are given in Table II. The combined effect of tempering temperature and time has been represented by the Grange and Baughman tempering parameter (TP), $T(14.44 + \log t)$, where 'T' is the tempering temperature in degree Kelvin and 't' is the tempering time in seconds.[34] Both yield strength and ultimate tensile strength of the samples decrease continuously with TP. The tensile ductility for all the samples is similar and is in the range of 12 to 15 pct. The fracture toughness first increases with TP and then decreases, with a maximum at a TP of 14,515 corresponding to the sample tempered at 768 K (495 °C) for 8 hours. The lower strength for this sample compared to the one tempered at the same temperature but for 4 hours indicates that this sample is overaged with respect to time. Minimum yield and tensile strengths, as well as a lower K_{IC}, were observed at a TP of 14,798 for the sample tempered at 783 K

Table II. Mechanical Properties of the Experimental UHS Steel Austenitized at 1173 K (900 °C) for Different Tempering Conditions

Tempering Condition (Temp/Time)	T (14.44 + $\log_{10} t$)*	Yield Strength (MPa)	UTS (MPa)	Elongation (pct)	K_{IC} (MPa$\sqrt{m}$)
758 K (485 °C)/4 h	14098	1855	2105	12.6	45.0
758 K (485 °C)/8 h	14326	1825	2040	13.4	66.0
768 K (495 °C)/4 h	14284	1825	2050	14.0	60.0
768 K (495 °C)/8 h	14515	1775	2030	15.0	87.0
783 K (510 °C)/8 h	14798	1600	1765	15.2	69.0

*Grange and Baughman tempering parameter.[34]

(510 °C) for 8 hours. This sample is overaged with respect to *both* temperature and time.

B. *Microstructural Characterization*

SEM and TEM studies on the as-quenched samples and the samples tempered at 768 K and 783 K (495 °C and 510 °C) showed microstructural features similar to those reported earlier for 758 K (485 °C) tempered samples.[14] The as-quenched sample (Figure 1a) shows a typical lath martensitic microstructure. Upon tempering in the range of 723 to 873 K (450 to 600 °C), it has been reported that fine needle-shaped M_2C precipitates are formed, predominantly on the dislocations. Many of these precipitates have sizes less than 5 nm, often less than 2 nm. It is well known[3] that it is difficult to observe these precipitates in optimally aged or slightly overaged conditions of these SHUHS steels in the TEM due to high dislocation density of the matrix. However, it is in general accepted[3] that the precipitates are needle shaped and have specific orientation relationships with the matrix. The identification of the precipitates and their morphology are usually confirmed by overaging the samples for longer times to coarsen the precipitates besides reducing the matrix dislocation density considerably. Figures 1(b) and (c) shows typical bright-field image and the corresponding [001] matrix zone axis pattern for the sample tempered at 768 K (495 °C) for 8 hours. Some of the more visible M_2C precipitates are indicated with arrows (Figure 1(b)). Our earlier work[14] and other literature[25] on SHUHS steels have shown that not only are still finer precipitates present, but also several 'clusters' comprising at times as few as 10-30 atoms. 3D atom probe is an ideal tool for investigating such clusters. The main focus of the work reported here is the atom probe characterization of clusters in the samples tempered at 768 K (495 °C) for 4 or 8 hours or 783 K (510 °C) for 8 hours.

1. *Establishing the presence of clusters*

The presence of clusters can be investigated by comparing observed solute atom frequency distributions to those of an ideal random solid solution with the same overall solute concentration as in the analyzed volume. In the latter case, one would expect a binomial distribution with the overall solute concentration as the "mean" of the distribution. In the event of segregation/clustering, deviations from the binomial distribution are expected. Figure 2 shows the experimental distribution of the carbide-forming elements (C, Cr, and Mo) compared to the respective binomial distributions for the random solid solution in the as-quenched sample. For this analysis, a block volume equivalent to 100 ions has been used. As the total number of ions in the analyzed volume was ~0.5 M, there were a total of 3620 blocks in the analyzed volume. Frequency distribution plots for carbon (Figure 2(a)) clearly reveal that the observed distribution for carbon is significantly different from the binomial distribution—for example, there are 1400 blocks with zero apct carbon in the observed distribution as compared to only 700 in the random distribution; in general, there are more blocks in the observed distribution than the random distribution for carbon contents either less than 1 apct or greater than 4 apct. Between these two values, the number of blocks in the observed distribution is less than that of the random one. This suggests that C atoms have already clustered in the as-quenched condition, which can also be confirmed from the corresponding atom map (Figure 3(a)). These results are consistent with the presence of carbon clusters identified by field-ion microscopy,[35] in the as-quenched medium carbon secondary hardening steel. In contrast, the observed distributions for Mo and Cr are nearly identical to the respective random binomial distributions suggesting negligible clustering for these two elements in the as-quenched condition (Figures 2(b) and (c)). This is also supported by the respective atom maps (Figures 3(b)

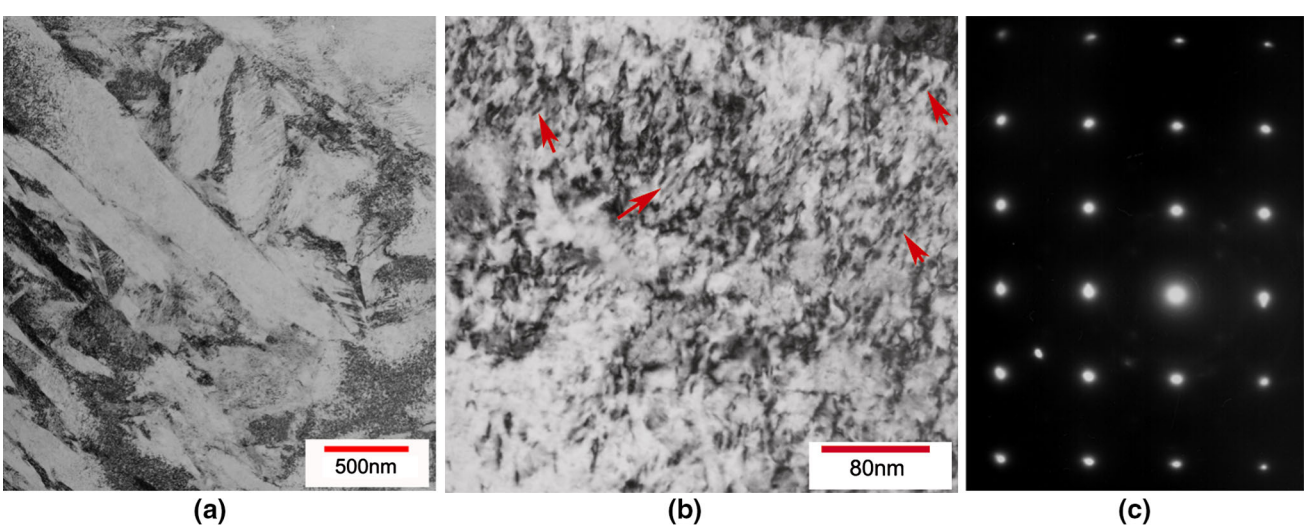

Fig. 1—(*a*) Bright-field TEM image for the as-quenched sample showing the presence of typical lath martensitic microstructure, (*b*) TEM bright-field image of the sample tempered at 768 K (495 °C) for 8 h showing the presence of M_2C precipitates indicated by arrows and (*c*) [001] martensite zone axis selected area diffraction pattern.

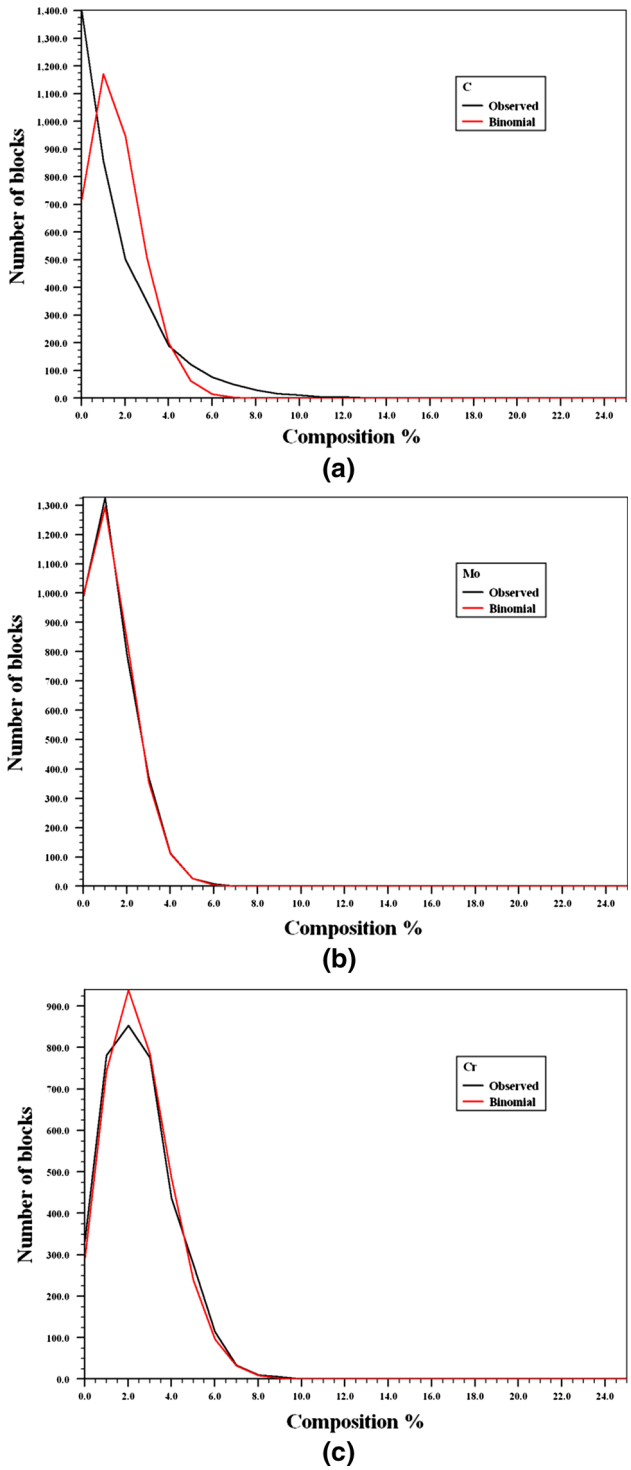

Fig. 2—Comparison of experimental and binomial distribution in the as-quenched sample: (*a*) carbon, (*b*) molybdenum, and (*c*) chromium (Color figure online).

and (c)). It must be noted that atom maps are less likely to capture the very early stages of clustering and comparison of observed and random binomial distributions is more reliable. Such a comparison shows no evidence of clustering for all the alloying elements (Cr, Mo, V, Co, and Ni) other than carbon.

However, the alloying elements Cr and Mo exhibit clear indications of clustering on tempering. For the sample tempered at 768 K (495 °C) for 8 hours, the observed frequency distributions for Cr and Mo are distinctly different from the random binomial distribution (Figures 4(a) and (b)), with chromium showing a larger deviation than molybdenum. These results are also similar to those observed by Mulholland and Seidman in the case of high-strength low-carbon steel.[36] Interestingly, V does not show any evidence of clustering (Figure 4(c)). As expected, the distribution for carbon shows stronger departure (Figure 4(d)) from the random distribution as compared to the as-quenched sample (Figure 2(a)). Individual atom maps (Figures 5(a) through (d)) reveal strong co-clustering of carbon, chromium, and molybdenum and negligible clustering of vanadium, consistent with the binomial distribution analysis. These observations are also in agreement with the relative diffusivities of C, Cr, Mo, and V in BCC Fe matrix.[37] C, being an interstitial atom, has highest diffusivity in BCC Fe, and Cr has the highest diffusivity among the substitutional solute elements, *i.e.*, Cr, Mo, and V present in this steel. As a result, during initial stages of tempering, at lower temperatures [<773 K (<500 °C)], Cr-rich carbides are expected to form. Mo-rich carbides might form when the steels are tempered at much higher temperatures.[37]

Similar analyses carried out on all tempered samples confirmed the presence of clusters in every sample investigated. A semi-quantitative analysis of the clusters, as a function of tempering condition, was attempted as described below.

2. *Identification of clusters and their analyses*

As mentioned earlier, after establishing the presence of clusters, maximum separation envelope method (MSEM) was employed for delineating the clusters to facilitate semi-quantitative statistical analyses of their size and composition, both of which have been determined from the constituent ions (atoms) identified to be part of the clusters. Figure 6 illustrates the delineation of clusters from the random solid solution in the sample tempered at 768 K (495 °C) for 4 hours. In the overall atom map (Figure 6(a)), it is rather difficult to identify the presence of clusters. However, on application of the MSEM and by displaying only atoms that have been identified as belonging to clusters, the presence of the latter is immediately obvious (Figure 6(b)). It should be noted that Figure 6 itself is a selected sub-volume, containing about 0.13 million ions, of a larger dataset comprising 0.3 million ions.

a. Cluster size analysis. The average size of the clusters in the different samples is summarized in Table III and depicted graphically in Figure 7. As expected, for a given tempering temperature [either 758 K or 768 K (485 °C or 495 °C)], the clusters coarsen with tempering time. The rate of coarsening of the clusters, as given by slope of the straight lines joining the data points for 4 and 8 hours of tempering, is higher for tempering at 758 K (485 °C) than at 768 K (495 °C). For a given time

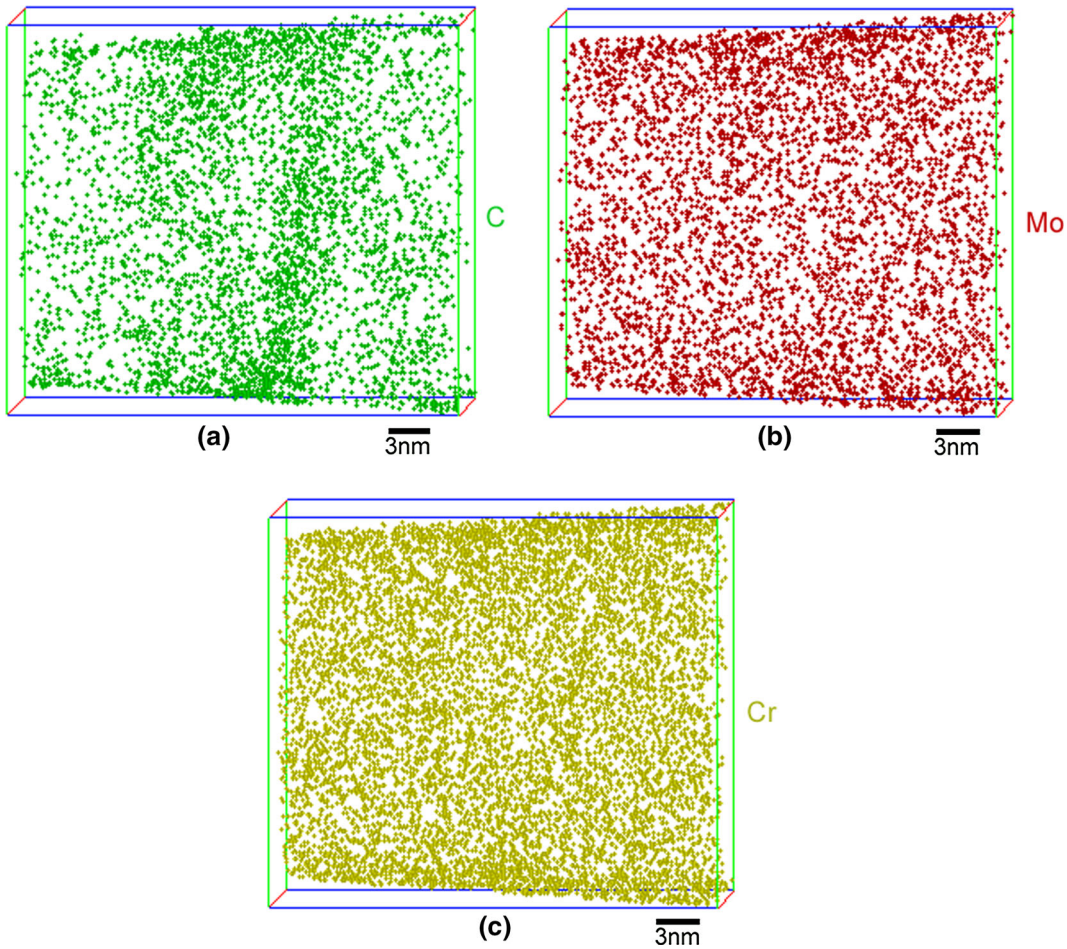

Fig. 3—Atom maps in the as-quenched sample for (*a*) carbon, (*b*) molybdenum, and (*c*) chromium, revealing C clustering, while Cr and Mo are in random solid solution (Color figure online).

(4 or 8 hours) at tempering temperature, the average size at 768 K (495 °C) is higher than the corresponding size at 758 K (485 °C). The average cluster size for the samples tempered at either 758 K or 768 K (485 °C or 495 °C) ranges from 1.10 to 1.34 nm. Clear coarsening is evident at the higher tempering temperature of 783 K (510 °C), with an average size of 2.26 nm, an increase of ~65 pct over the average cluster size of other samples. All the above observations are in agreement with the expected kinetics.

To facilitate more detailed analyses, we have compared the size distribution of clusters in different samples. The cluster size distribution, for the sample showing the maximum fracture toughness (tempered at 768 K (495 °C) for 8 hours) and the one overaged with respect to both temperature and time (tempered at 783 K (510 °C) for 8 hours), is shown in Figure 8. In the 768 K (495 °C) tempered sample, just over 85 pct of the clusters detected had a diameter between 0.8 and 1.6 nm, and 90 pct of the clusters had a diameter less than 2 nm. Only ~2 pct of the clusters had a diameter larger than 4 nm. It should be noted that the probability of observing such large clusters (or *fine* precipitates) in a conventional 3DAP with a field of view of 10 × 10 nm is quite small. While the 783 K (510 °C) tempered sample shows rather similar behavior overall, the cumulative percentage frequency (not shown) indicates the presence of a larger fraction of clusters with larger sizes than in 768 K (495 °C) tempered sample, especially those with size >2.8nm.

b. Cluster composition analysis. Composition of all the clusters can be best represented in the form of stack plots[14,29] such as the one shown in Figure 9 for the sample tempered at 768 K (495 °C) for 8 hours. The data have been plotted in terms of increasing carbon content. Clusters, here, have been divided into two categories based on their carbon content. Clusters with less than 10 apct carbons are designated as carbon deficient and those with greater than 10 apct carbon as carbon rich. This distinction while somewhat arbitrary also has a certain basis: the carbide with lowest carbon content reported in this class of steels is M_6C (Table IV), which contains nearly 14 apct carbon. Thus, using 10 apct as the limit to distinguish between carbon-deficient and carbon-rich clusters appears reasonable. Figures 9(a) and (b) shows the composition of the carbon-deficient and carbon-rich clusters, respectively. The concentrations of Cr, Mo, and Fe show a wide variation, ranging from 5 to 50 apct. As we have

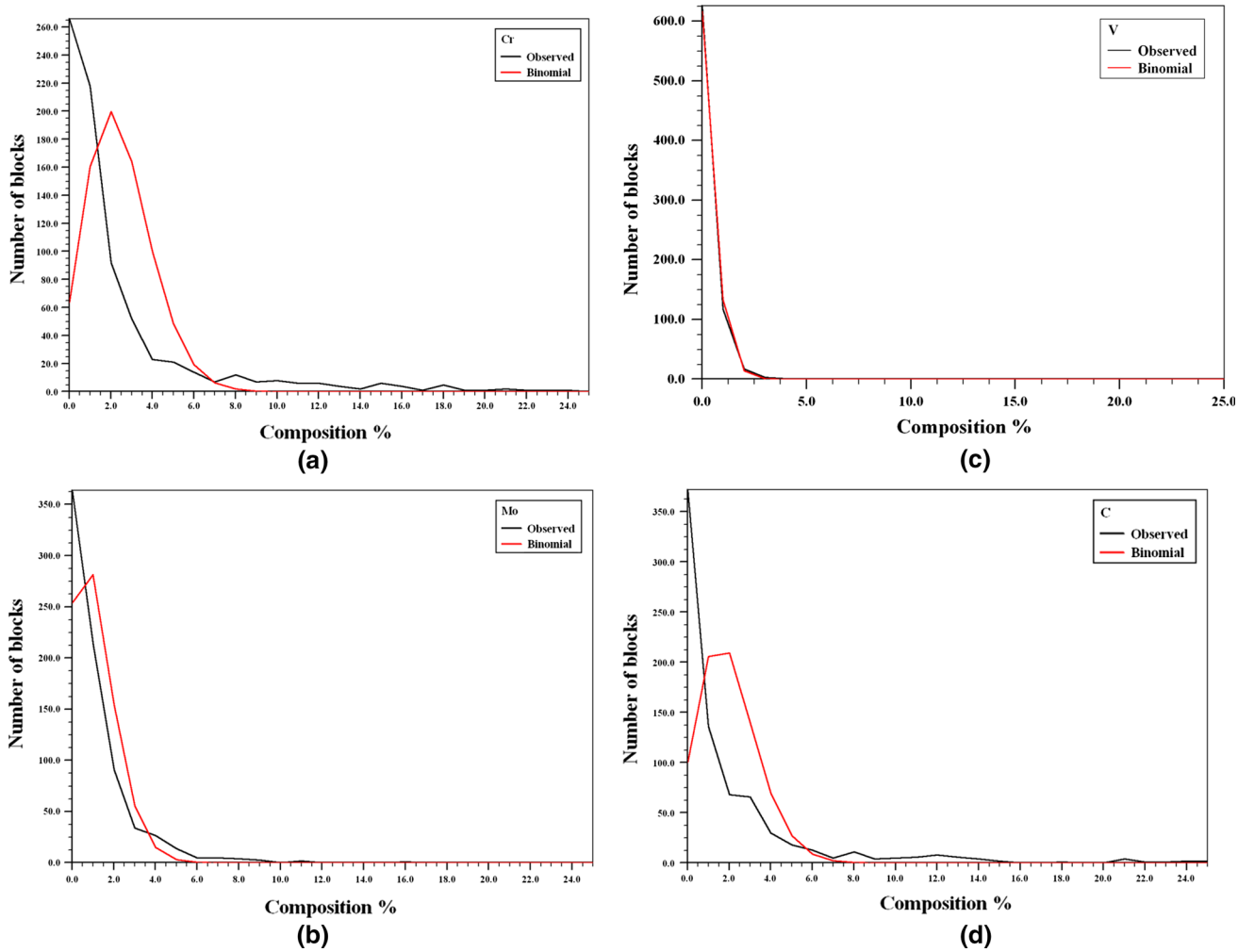

Fig. 4—Comparison of experimental and binomial distributions in the sample tempered at 768 K (495 °C) for 8 h: (*a*) chromium, (*b*) molybdenum, (*c*) vanadium, and (*d*) carbon (Color figure online).

reported earlier,[14] key factors for the large variation are the small size of the clusters (which implies that every single atom contributes significantly to the composition) and the inherent nature of the particle detection algorithm. The cluster composition data for all samples are summarized in Table V. Average carbon content of the carbon-deficient and carbon-rich clusters is ~5 to 6 and 16 to 18 apct, respectively, for the different samples. Cr content of both types of clusters decreased almost continuously from the sample tempered at 758 K (485 °C) for 4 hours to the sample tempered at 783 K (510 °C) for 8 hours. However, such patterns do not seem to exist for Fe and Mo contents. The mean values of the other carbide-forming element V and matrix elements Co and Ni were found to vary in the range of 2 to 3, 4 to 6, and 5 to 7 apct, respectively, quite similar to their respective levels in the surrounding matrix, suggesting that they do not participate in the clustering process. Hence, these elements are not included in Table V. From the table, it can be seen that carbon-deficient clusters have slightly higher Cr and Mo and significantly higher Fe contents relative to carbon-rich clusters. In general, the clusters appear to contain a significant amount of Fe (26 to 34 apct) in all the heat treatment conditions. There are two likely reasons for this: (a) deficiencies in the cluster detection algorithm resulting in the surrounding matrix atoms being counted as part of the cluster, and (b) iron, the matrix element is also a reasonably strong carbide former, and hence the clusters initially form with higher Fe content. By performing sensitivity analyses with respect to the various parameters used in the cluster detection algorithm, it has been established that the former is less likely, leaving the latter as the primary cause of the observed iron content of the clusters. These results are broadly in agreement with those reported by Liu *et al.*[17] in the case of multi-component V-Nb micro-alloyed steel in which they found the iron content of 3.5 to 5 nm clusters to be as high as 60 apct. In these clusters, the amounts (in apct) of other elements were reported to be 15.7 ± 1.3C, 16.7 ± 1.3V, 4.2 ± 0.7Nb, and 1.3 ± 0.4Mo.

The frequency distribution of the carbon content of the clusters for the samples, tempered for 8 hours at 768 K or 783 K (495 °C or 510 °C), shows striking differences, especially for carbon content up to about

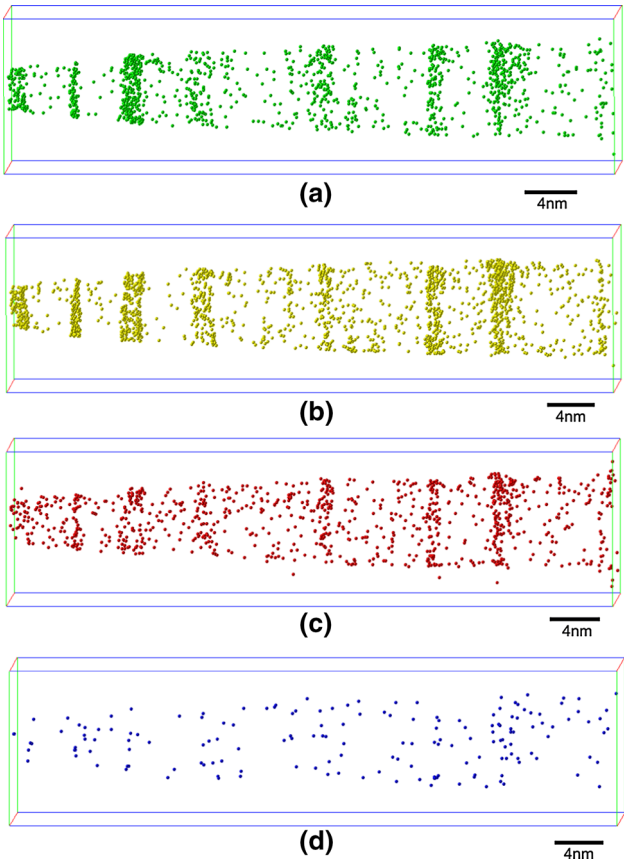

Fig. 5—Atom maps for the sample tempered at 768 K (495 °C) for 8 hours: (*a*) carbon, (*b*) chromium, (*c*) molybdenum, and (*d*) vanadium (Color figure online).

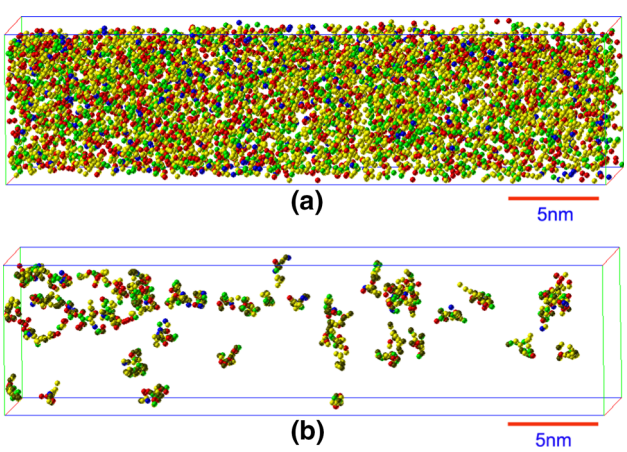

Fig. 6—Illustration of delineation of clusters from random solid solution; (*a*) before the application of MSEM showing random distribution of C, Cr, Mo, and V and (*b*) after the application of MSEM showing those C, Cr, Mo, V, and Fe atoms identified as belonging to clusters. Color key: Fe-olive green, C-parrot green, Cr-yellow, Mo-red, and V-blue (Color figure online).

Table III. Average Size of the Clusters/Precipitates as a Function of Tempering Condition

Heat Treatment Condition (Tempering Temperature/Time)	T (14.44 + $\log_{10} t$)*	Average Cluster Size (nm)#
758 K (485 °C)/4 h	14098	1.10 ± 0.03
758 K (485 °C)/8 h	14326	1.22 ± 0.06
768 K (495 °C)/4 h	14284	1.27 ± 0.02
768 K (495 °C)/8 h	14515	1.34 ± 0.03
783 K (510 °C)/8 h	14798	2.26 ± 0.04

*Grange and Baughman tempering parameter.[34]
#Data given as mean ± standard error.

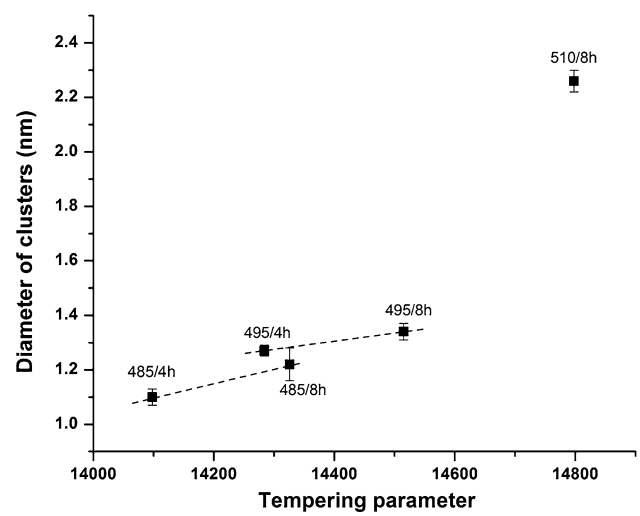

Fig. 7—Variation of cluster diameter as a function of tempering parameter.

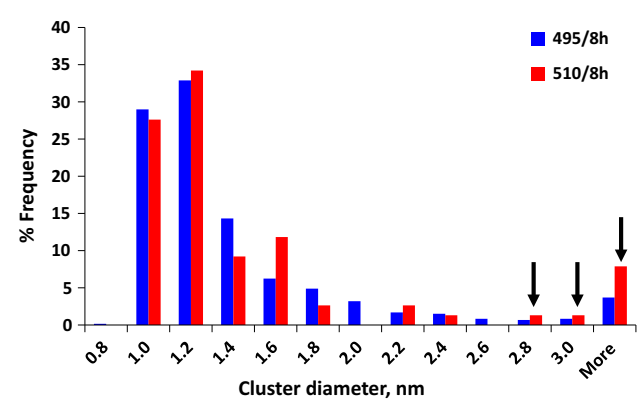

Fig. 8—Comparison of percentage frequency histograms as a function of diameter of clusters for the samples tempered at 768 K and 783 K (495 °C and 510 °C) for 8 h (Color figure online).

30 apct (Figure 10). In the 768 K (495 °C) tempered sample, the clear dominance of clusters with carbon content less than 15 apct is quite evident, as they account for more than 70 pct of the total clusters observed. In comparison, only about 50 pct of the clusters have less than 15 apct in the 783 K (510 °C) tempered sample. If we consider carbon content less than 10 apct, the amounts of clusters in the two samples are 46 and 26 pct, respectively. Thus, it can be surmised that the frequency distribution shifts toward higher carbon content for the sample tempered at 783 K (510 °C).

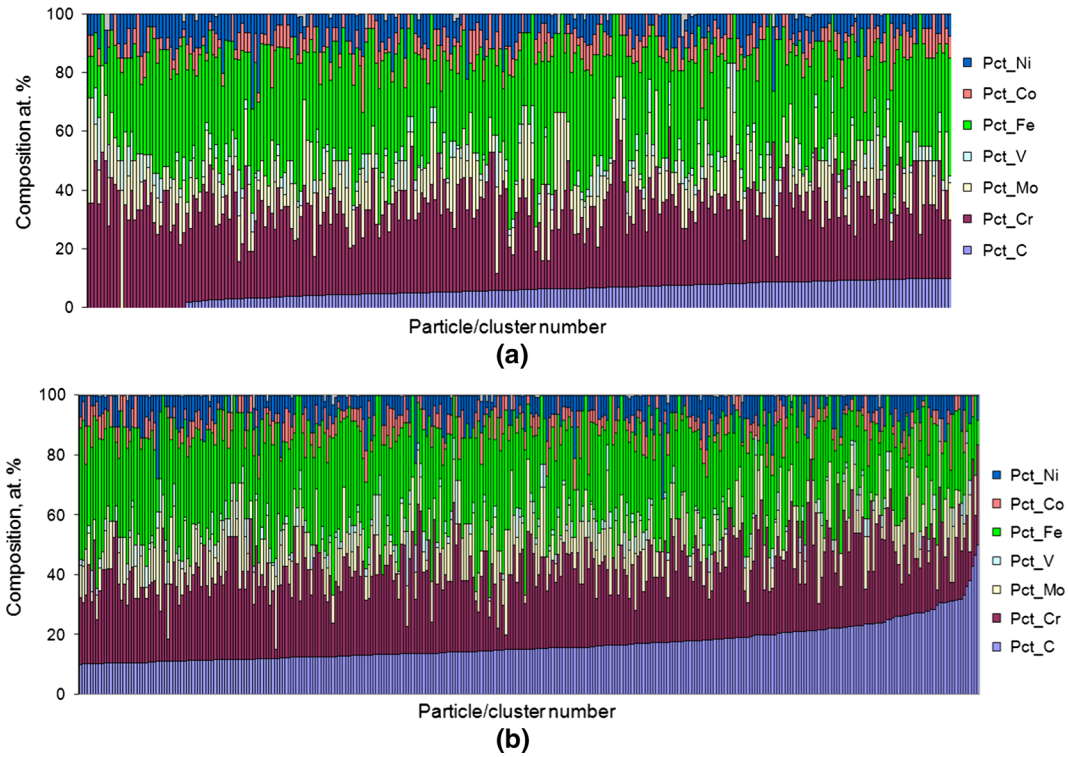

Fig. 9—Stack plots showing the composition of individual clusters in the sample tempered at 768 K (495 °C) for 8 h: (*a*) carbon-deficient and (*b*) carbon-rich clusters (Color figure online).

Table IV. Common Carbides Observed in SHUHS Steels

Formula	M_6C	$M_{23}C_6$	M_2C	M_7C_3
Atom pct C	14.28	20.68	33.33	30.00
Number of atoms in unit cell	112	116	4	40

Table V. Composition in apct (Mean ± Standard Error) of Carbon-Deficient and Carbon-Rich Clusters Along with Overall Composition of the Clusters

HT Condition	C	Cr	Mo	Fe
Carbon-deficient clusters				
758 K (485 °C)/4 h	5.92 ± 0.55	32.29 ± 1.64	17.78 ± 1.32	30.48 ± 1.34
758 K (485 °C)/8 h	5.53 ± 0.58	30.06 ± 1.80	20.94 ± 1.70	32.46 ± 2.01
768 K (495 °C)/4 h	6.13 ± 0.18	28.15 ± 0.59	12.98 ± 0.43	37.02 ± 0.58
768 K (495 °C)/8 h	5.82 ± 0.18	29.68 ± 0.56	14.34 ± 0.46	33.48 ± 0.56
783 K (510 °C)/8 h	5.62 ± 0.79	26.04 ± 2.39	18.50 ± 2.30	35.22 ± 2.02
Carbon-rich clusters				
758 K (485 °C)/4 h	17.88 ± 0.69	30.73 ± 1.11	13.66 ± 0.86	24.91 ± 0.97
758 K (485 °C)/8 h	18.20 ± 0.75	28.07 ± 1.01	18.51 ± 0.94	24.86 ± 1.32
768 K (495 °C)/4 h	16.60 ± 0.28	25.71 ± 0.48	11.73 ± 0.39	31.82 ± 0.51
768 K (495 °C)/8 h	16.90 ± 0.34	27.23 ± 0.50	12.98 ± 0.38	28.90 ± 0.53
783 K (510 °C)/8 h	18.33 ± 0.77	20.64 ± 1.38	19.18 ± 1.23	29.00 ± 1.29
All clusters				
758 K (485 °C)/4 h	14.43 ± 0.73	31.18 ± 0.92	14.85 ± 0.74	26.52 ± 0.82
758 K (485 °C)/8 h	14.45 ± 0.81	28.66 ± 0.89	19.23 ± 0.83	27.11 ± 1.15
768 K (495 °C)/4 h	12.18 ± 0.28	26.74 ± 0.38	12.26 ± 0.29	34.02 ± 0.40
768 K (495 °C)/8 h	11.95 ± 0.31	28.32 ± 0.38	13.59 ± 0.30	30.95 ± 0.39
783 K (510 °C)/8 h	14.98 ± 0.88	22.06 ± 1.22	19.00 ± 1.08	30.64 ± 1.13

HT refers to heat treatment.

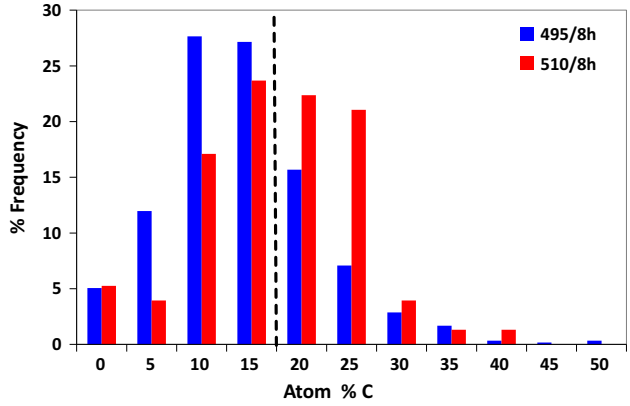

Fig. 10—Comparison of percentage frequency histograms as a function of carbon content of clusters for the samples tempered at 768 K and 783 K (495 °C and 510 °C) for 8 h (Color figure online).

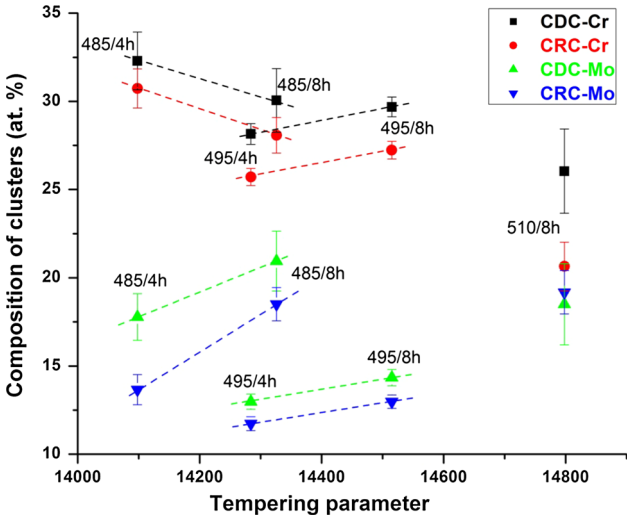

Fig. 11—Variation of Cr and Mo concentrations in carbon-rich (CRC) and carbon-deficient clusters (CDC) with respect to tempering parameter (Color figure online).

Compositional analysis for Cr and Mo in the carbon-deficient as well as carbon-rich clusters has been performed as a function of tempering treatment (Figure 11). With increase in tempering time, at 758 K (485 °C), Cr content decreases and Mo content increases, the latter more strongly, in both types of clusters. In contrast, at 768 K (495 °C), both Cr and Mo contents increase with tempering time, the latter slightly less than the former. Comparing the samples tempered for 4 hours at 758 K and 768 K (485 °C and 495 °C) reveals that Cr and Mo contents are significantly lower, in both types of clusters, in 768 K (495 °C) sample. This implies that Fe content of the clusters is the highest in the 768 K (495 °C)/4 hours sample, a fact also seen from Table V. Since the increase in Cr and Mo contents with increase in tempering time (8 *vs* 4 hours) is marginal in the 768 K (495 °C) samples, this suggests that significant amount of Fe remains in the clusters even after 8 hours of tempering. At 783 K (510 °C), the Cr and Mo contents are nearly equal (within limits of statistical error) for carbon-rich clusters, while the carbon-deficient clusters are clearly richer in Cr than Mo.

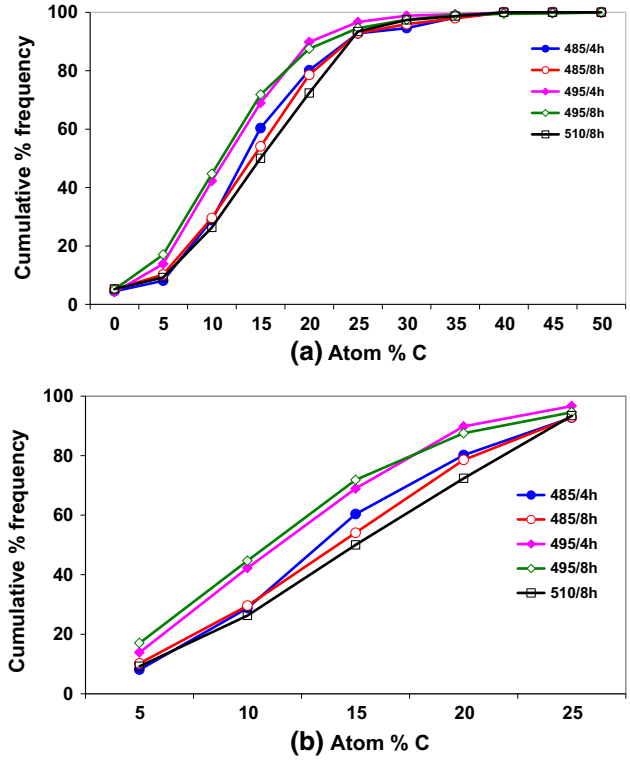

Fig. 12—Cumulative percentage frequency of clusters as a function of carbon content in different tempering conditions: (*a*) 0 to 50 apct carbon and (*b*) magnified plot of (a) showing between 5 and 25 apct C (Color figure online).

Cumulative percentage frequency distributions in terms of carbon content for all the five samples (Figure 12) show that for carbon content less than 25 apct, the samples tempered at 768 K (495 °C) behave differently from the samples tempered at either 758 or 783 K (485 or 510 °C). The former has a larger percentage of carbon-deficient clusters than the latter—more than 42 pct as opposed to ~26 to 30 pct of clusters with similar carbon content. In all cases, only a small percentage of clusters (3 to 8 pct) have carbon content greater than 25 at. pct. These observations are broadly in agreement with those reported by Carinci *et al.*[25] who, based on 1D atom probe analysis of tempered samples of AF1410 steel, have suggested that the clusters are sub-stoichiometric with respect to C at the normal tempering temperature of 783 K (510 °C) for 5 to 8 hours. They have further reported that even after 24 hours of aging at 783 K (510 °C), the particles appear to have a stoichiometry of $M_2C_{0.8}$.

3. *On the presence of carbon-deficient clusters*

In the present work, the presence of clusters has been proved in SHUHS steels in the peak-aged (TP: 14,098), optimally aged (TP: 14,284, 14,326, & 14,515), and overaged (TP: 14,798) conditions. These results are consistent with the presence of clusters in several alloy systems such as Al alloys,[20,21] Cu alloys,[23] and steels.[15,17-19,24] The clusters were divided into two

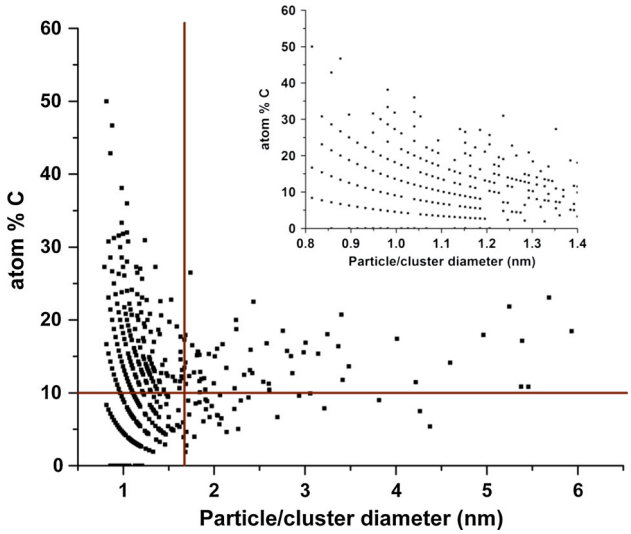

Fig. 13—Plot of apct carbon in clusters as a function of cluster size for 768 K (495 °C) tempered sample for 8 h; inset shows the enlarged view of the plot between particle diameter 0.8 and 1.4 nm.

categories: carbon-rich and carbon-deficient clusters. While the presence of the former might be expected, given that the reported strengthening precipitates in this class of steels are M_2C type carbides, one would normally expect the carbon-deficient (intermetallic) clusters to be present in steels strengthened by intermetallic precipitates, such as Ni_3Ti, NiAl, or Ni_3Mo as in the case of maraging steels,[19,24,35] stainless steels,[38] and low-alloy steels.[39] It is therefore interesting, and important, to examine whether the carbon-deficient clusters are precursors to carbides, or do they exist as a separate population? If the former is true, one would expect that at any given tempering condition, the smaller clusters are deficient in carbon and, with increasing size, the average carbon content of the clusters also increases. A plot of carbon content as a function of size (Figure 13) for the sample tempered at 768 K (495 °C) for 8 hours shows no such correlation; if any, a few of the smaller clusters (inset of Figure 13) seem to have carbon content greater than 30 at. pct. But, in these small clusters in which the total number of atoms is small, the individual atomic contribution to the cluster composition is significantly larger, thereby leading to high concentrations at times. For example, in a cluster with 10 atoms or 20 atoms (corresponding to cluster diameter of ~0.8 or 1 nm), each atom accounts for 10 or 5 pct, respectively. The apparent *discretization* and the *patterns* on which the individual points seem to lie (Figure 13) are a consequence of this fact. This effect diminishes at larger sizes because the individual atomic contribution (to the total) decreases as the size increases.

The average composition (in apct) of large clusters (>3 nm) was found to be 25.36Cr-11.57Mo-2.16V-38.28Fe-6.78Co-7.68Ni-7.93C. If all clusters were precursors to the formation of M_2C carbides, one would expect the carbon content of these clusters to approach ~33 apct. However, a significant number of carbon-deficient clusters (with <10 apct carbon) containing more than 100 atoms (corresponding to diameter

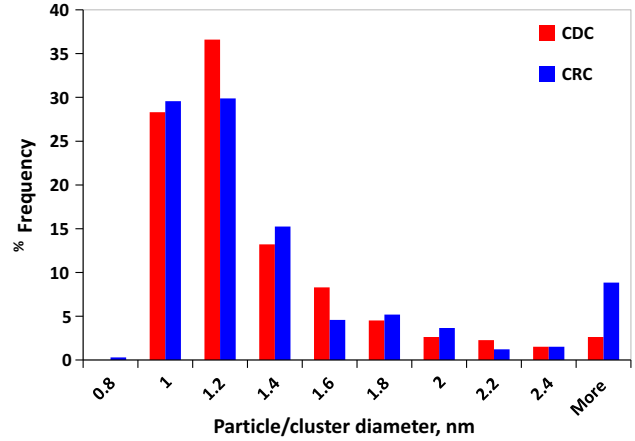

Fig. 14—Particle size distribution, in terms of percentage frequency of carbon-deficient (CDC) and carbon-rich clusters (CRC) for the sample tempered at 768 K (495 °C) for 8 h (Color figure online).

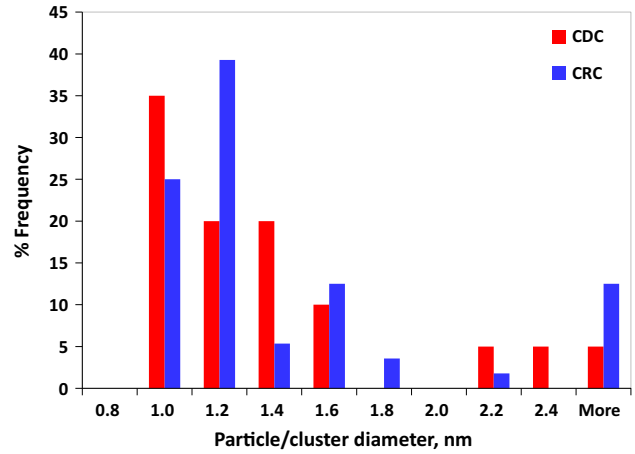

Fig. 15—Particle size distribution, in terms of percentage frequency of carbon-deficient (CDC) and carbon-rich clusters (CRC) for the sample tempered at 783 K (510 °C) for 8 h (Color figure online).

~1.65 nm) are also seen. This suggests that the carbon-deficient clusters exist as a population distinct from the carbon-rich clusters. This can also be ascertained from frequency distribution plots for carbon-deficient and carbon-rich clusters (Figure 14). It is seen that both types of clusters show a similar distribution and both have a peak at 1.2 nm. The cumulative distribution (not shown) confirms that, on the average, carbon-deficient clusters tend to be smaller than the carbon-rich clusters. Similar plots for samples in other tempering conditions, such as those for the sample tempered at 783 K (510 °C) for 8 hours (Figure 15), also show the same behavior with only minor shifts in the position of the peaks. Figure 15 clearly shows the presence of a reasonable fraction of carbon-deficient clusters with size greater than 2 nm coexisting with carbon-rich clusters of similar size. This reaffirms that the carbon-deficient clusters do exist as a separate population under the tempering conditions investigated in this study.

So, the question arises as to why these carbon-deficient clusters exist? Normally, it is assumed that the

formation of secondary hardening precipitates [which occurs at temperatures above ~673 K (~ 400 °C)] in this class of UHS steels is limited by the diffusion of the substitutional carbide-forming solutes as carbon can freely diffuse at these temperatures. Given that the steel under investigation contains 0.37 wt pct. carbon, it appears that neither the availability nor the diffusivity of carbon is responsible for the presence of carbon-deficient clusters which cannot therefore be explained on the basis of kinetics. This would suggest that these clusters are at least metastable (in a thermodynamic sense) under the conditions investigated. If this is so, there is an even higher likelihood of such clusters being present in classical secondary hardening UHS steels such as HY180, AF1410, or AerMet100. This is because there is a lesser amount of carbon present relative to the amount of carbide-forming elements (Cr and Mo) in these steels than in the experimental UHS steel. This can be quantified using C/M ratio, where C and M refer to the concentration in atomic percent of carbon and carbide-forming elements, respectively. This ratio in the experimental UHS steel is 0.58, whereas the C/M ratio is 0.18, 0.27, and 0.34 for HY180, AF1410, and AerMet100, respectively. Therefore, it is probable that considerable amounts of carbon-deficient clusters are present in these steels as well. However, this needs to be ascertained experimentally.

4. *Effect of clusters on mechanical properties*

From atom probe data, an indication of the volume fraction of the clusters can be obtained from the ratio of total number of atoms identified as being in the clusters to the overall number of atoms in the analyzed volume. Our observations suggest that clusters constitute between 1.14 and 2.53 vol pct of the microstructure, under the different conditions investigated.

The clusters might have a significant effect on the mechanical properties of these secondary hardening UHS steels. While there are no other reports in the literature about the presence of clusters in secondary hardening steels, the available literature on cluster strengthening mechanisms in other steels, aluminum, and copper alloys[19,24,40-46] suggests that the most significant contributions arise from modulus hardening and order strengthening. The former arises due to the change in the shear modulus locally in the vicinity of clusters.[41] When a dislocation approaches a region with different modulus, it will either be repelled if the modulus is higher or attracted when the modulus of the region is lower. Both these effects need extra energy to move the dislocation, resulting in additional strengthening.[47] In contrast, order strengthening arises from the extra energy that is required for dislocations to cut a diffuse anti-phase boundary formed by the clusters.[19] The authors of that study have indicated that this mechanism of hardening also has the potential to produce the maximum toughness, as the presence of clusters provides a network of elastically soft and relatively diffuse anti-phase boundaries as obstacles for the movement of dislocations. When a dislocation cuts an elastically soft precipitate, the tendency for the formation of dislocation pileups is minimum, thereby enhancing the toughness. This study was performed on maraging steels in which all the precipitates are ordered intermetallics such as Ni_3Ti. In the secondary hardening steels, it is likely that the latter mechanism is more dominant for the carbon-deficient clusters (which resemble intermetallics) than for the carbon-rich clusters. Indeed, in our study, we have found that the sample with maximum amount (~45 pct) of carbon-deficient clusters also has the maximum toughness [the one tempered at 768 K (495 °C) for 8 hours]. However, it is not clear why the sample tempered at 768 K (495 °C) for 4 hours, in which ~42 pct of the clusters are carbon deficient, does not exhibit good toughness; perhaps, other mechanisms, which account for the high UTS in this sample, are also responsible for the concomitant poor toughness.

IV. CONCLUSIONS

The present study was undertaken to investigate, using 3D atom probe, clusters in a medium carbon secondary hardening ultra-high-strength steel austenitized at 1173 K (900 °C) for 1 hour and tempered at 758 K, 768 K, or 783 K (485 °C, 495 °C, or 510 °C) for 4 or 8 hours. In terms of mechanical properties, the sample tempered at 758 K (485 °C) for 4 hours exhibited the maximum yield and tensile strength levels and minimum toughness, while the sample tempered at 783 K (510 °C) for 8 hours has shown minimum yield and tensile strength levels and intermediate toughness. Optimum combination of strength and toughness has been achieved in the sample tempered at 768 K (495 °C) for 8 hours. The main conclusions from the atom probe study are as follows:

1. The presence of clusters could be unambiguously established by comparing the observed spatial distribution of the different alloying elements against the corresponding distribution expected for a random solid solution. Analysis of these statistical distributions for the different solute elements has revealed that only carbon exhibits clustering even in the as-quenched condition, whereas Cr and Mo show clustering in all tempered conditions. Significant clustering was not observed for Co, Ni, or V. These observations were further confirmed by examining atom maps.
2. The clusters were found to constitute a significant fraction, between 1.14 and 2.53 vol pct, of the microstructure in the different tempered conditions.
3. In general, as expected, the size of clusters/precipitates increased with both tempering temperature and tempering time. The rate of coarsening at 758 K (485 °C) with time was found to be higher than that at 768 K (495 °C). Considering isochronal tempering for 8 hours as a function of tempering temperature, substantial coarsening of the clusters was observed after tempering at 783 K (510 °C) with an average size of 2.26 nm, compared to ~1.1 nm at 758 K or 768 K (485 °C or 495 °C).
4. In terms of composition, on the average, the carbon content remained fairly constant between 12 and

15 apct irrespective of the tempering condition. In contrast, the Cr content was found to decrease upon increase of either tempering temperature or time. Mo and Fe did not show any such uniform pattern.

5. The clusters were broadly divided into two categories based on their carbon content, namely carbon-rich as well as carbon-deficient clusters. In the samples tempered for 8 hours, the amount of carbon-deficient clusters decreased significantly, from 45 pct at 768 K (495 °C) to 26 pct at 783 K (510 °C), accompanied by a proportionate increase in carbon-rich clusters.
6. In general, no clear correlation could be observed between size and carbon content of the clusters for any of the tempering conditions investigated. However, for clusters containing more than ~100 atoms, the proportion of carbon-rich clusters was always found to be higher than that of the carbon-deficient clusters. Nevertheless, the presence of even a few large clusters of the latter category suggests that they (carbon-deficient clusters) form a separate population and are not necessarily precursors to equilibrium carbide precipitates.

The current study has unambiguously established the presence of clusters, especially carbon-deficient clusters, in an experimental SHUHS steel in underaged, peak-aged, and overaged conditions. As the experimental steel has a higher C/(Cr + Mo) ratio of 0.58 relative to standard SHUHS steels such as HY180, AF1410, and AerMet100 which have C/(Cr + Mo) ratio in the range of 0.18 to 0.34, the possibility of the presence of carbon-deficient clusters in the latter steels is much higher and merits investigation. Clusters, in general, and carbon-deficient ones, in particular, could exert a significant influence on mechanical properties of this important class of steels and offer the potential to engineer the microstructure through heat treatment to achieve an optimal combination of strength and toughness.

ACKNOWLEDGMENTS

This research was funded by the Defence Research and Development Organization (DRDO), India. The permission of the Director, Defence Metallurgical Research Laboratory (DMRL), Hyderabad, to publish the results is gratefully acknowledged. The authors wish to thank Professor W. M. Garrison, Jr., Department of Materials Science and Engineering, Carnegie Mellon University, Pittsburgh, The USA, for useful discussions, and Dr. G. Malakondaiah, former Director, DMRL and former Chief Controller R&D at DRDO Headquarters, for his constant encouragement.

REFERENCES

1. G.R. Speich, D.S. Dabkowski, and L.F. Porter: *Metall. Trans.*, 1973, vol. 4, pp. 303–15.
2. R. Ayer and P.M. Machmeier: *Metall. Mater. Trans. A*, 1996, vol. 28A, pp. 2510–18.
3. R. Ayer and P.M. Machmeier: *Metall. Trans. A*, 1993, vol. 28A, pp. 1943–55.
4. J.M. Dahl and P.M. Novotny: *Adv. Mater. Process.*, 1999, vol. 155, pp. 23–25.
5. Z. Hu, X. Wu, and C. Wang: *J. Mater. Sci. Technol.*, 2004, vol. 20, pp. 425–28.
6. M. Grujicic: *CALPHAD*, 1990, vol. 14, pp. 49–59.
7. L.E. Iorio, J.L. Maloney, and W.M. Garrison, Jr.: *40th Mechanical Working and Steel Processing Conf. Proc., Vol. XXXVI, ISS-AIME*, Warrendale, PA, 1999, pp. 901–20.
8. H.R. Yang, K.B. Lee, and H. Kwon: *Metall. Mater. Trans. A*, 2001, vol. 32A, pp. 2393–96.
9. K.S. Cho, J.H. Choi, H.S. Kang, S.H. Kim, K.B. Lee, H.R. Yang, and H. Kwon: *Mater. Sci. Eng. A*, 2010, vol. 527, pp. 7286–93.
10. J.S. Montgomery and G.B. Olson: *Proc. G.R. Speich Symp.,* G. Krauss and P.E. Repas, eds., ISS, Warrendale, PA, 1992, pp. 177–214.
11. P.M. Machmeier, T. Matuszewski, R. Jones, and R. Ayer: *J. Mater. Eng. Perf.*, 1997, vol. 6, pp. 279–88.
12. K. Stiller, L.-E. Svensson, P.R. Howell, W. Rong, H.-O. Andren, and G.L. Dunlop: *Acta Mater.*, 1984, vol. 32, pp. 1458–68.
13. J. Akre, F. Danoix, H. Leitner, and P. Auger: *Ultramicroscopy*, 2009, vol. 109, pp. 518–23.
14. R. Veerababu, R. Balamuralikrishnan, K. Muraleedharan, and M. Srinivas: *Metall. Mater. Trans. A*, 2008, vol. 39A, pp. 1486–95.
15. K.Y. Xie, T. Zheng, J.M. Cairney, H. Kaul, J.G. Williams, F.J. Barbaro, C.R. Killmore, and S.P. Ringer: *Scripta Mater.*, 2012, vol. 66, pp. 710–13.
16. E.V. Pereloma, I.B. Timokhina, K.F. Russell, and M.K. Miller: *Scripta Mater.*, 2006, vol. 54, pp. 471–76.
17. Q.D. Liu, W.Q. Liu, and S.J. Zhao: *Metall. Mater. Trans. A*, 2011, vol. 42A, pp. 3952–60.
18. S.L. Shrestha, K.Y. Xie, C. Zhu, S.P. Ringer, C. Killmore, K. Carpenter, H. Kaul, J.G. Williams, and J.M. Cairney: *Mater. Sci. Eng. A*, 2013, vol. 568, pp. 88–95.
19. E.V. Pereloma, A. Shekhter, M.K. Miller, and S.P. Ringer: *Acta Mater.*, 2004, vol. 52, pp. 5589–5602.
20. G. Sha, R.K.W. Marceau, X. Gao, B.C. Muddle, and S.P. Ringer: *Acta Mater.*, 2011, vol. 59, pp. 1659–70.
21. G. Sha, H. Moller, W.E. Stumpf, J.H. Xia, G. Govender, and S.P. Ringer: *Acta Mater.*, 2012, vol. 60, pp. 692–701.
22. N. Stanford, G. Sha, A. La Fontaine, M.R. Barnett, and S.P. Ringer: *Metall. Mater. Trans. A*, 2009, vol. 40A, pp. 2480–87.
23. Y. Aruga, D.W. Saxey, E.A. Marquis, H. Shishido, Y. Sumino, A. Cerezo, and G.D.W. Smith: *Metall. Mater. Trans. A*, 2009, vol. 40A, pp. 2888–2900.
24. A. Shekhter, H.I. Aaronson, M.K. Miller, S.P. Ringer, and E.V. Pereloma: *Metall. Mater. Trans. A*, 2004, vol. 35A, pp. 973–83.
25. G.M. Carinci, G.B. Olson, J.A. Liddle, L. Chang, and G.D.W. Smith: in G.B. Olson, M. Azrin, E.S. Wright, eds., *Innovations in Ultra High Strength Steel Technology, 34th Sagamore Army Materials Research Conference Proceedings*, U.S. Government Printing Office, Washington, DC, 1990, pp. 189-208.
26. M.K. Miller: *Atom Probe Tomography*, Kluwer Academic/Plenum Press, New York, 2000, pp. 28-34, 158-159.
27. R.K.W. Marceau, A. de Vaucorbeil, G. Sha, S.P. Ringer, and W.J. Poole: *Acta Mater*, 2013, vol. 61, pp. 7285–7303.
28. D. Vaumousse, A. Cerezo, and P.J. Warren: *Ultramicroscopy*, 2003, vol. 95, pp. 215–21.
29. M.K. Miller and K.F. Russell: *J. Nucl. Mater.*, 2007, vol. 371, pp. 145–60.
30. M.K. Miller, K.F. Russell, M.A. Sokolov, and R.K. Nanstad: *J. Nucl. Mater.*, 2008, vol. 351, pp. 248–61.
31. Y. Aruga and H. Nako: *Metall. Mater. Trans. A*, 2012, vol. 43A, pp. 1102–08.
32. I.B. Timokhina, M. Enomoto, M.K. Miller, and E.V. Pereloma: *Metall. Mater. Trans. A*, 2012, vol. 43A, pp. 2473–83.
33. J.M. Hyde, G. Sha, E.A. Marquis, A. Morley, K.B. Wilford, and T.J. Williams: *Ultramicroscopy*, 2011, vol. 111, pp. 664–71.
34. S.L. Semiatin, D.E. Stutz, and T.G. Byrer: *J. Heat Treat.*, 1985, vol. 4, pp. 39–40.

35. S.D. Erlach, H. Leitner, M. Bischof, H. Clemens, F. Danoix, D. Lemarchand, and I. Siller: *Mater. Sci. Eng. A*, 2006, vol. 429, pp. 96–106.
36. M.D. Mulholland and D.N. Seidman: *Acta Mater.*, 2011, vol. 59, pp. 1881–97.
37. H.K.D.H. Bhadeshia and R.W.K. Honeycombe: *Steels Microstructure and Properties*, 3rd ed., Elsevier Ltd., Linacre House, Jordan Hill, Oxford, UK, pp. 11, 12, 200.
38. Z. Guo, W. Sha, and D. Vaumousse: *Acta Mater.*, 2003, vol. 51, pp. 101–116.
39. J.M. Hyde, M.G. Burke, R.M. Boothby, and C.A. English: *Ultramicroscopy*, 2009, vol. 109, pp. 510–17.
40. R. Schnitzer, M. Schober, S. Zinner, and H. Leitner: *Acta Mater.*, 2010, vol. 58, pp. 3733–41.
41. M.J. Starink and S.C. Wang: *Acta Mater.*, 2009, vol. 58, pp. 2376–89.
42. E.A. Marquis and J.M. Hyde: *Mater. Sci. Eng. R*, 2010, vol. 69, pp. 37–62.
43. B. Timokhina, P.D. Hodgson, S.P. Ringer, R.K. Zheng, and E.V. Pereloma: *Mater. Sci. Technol.*, 2011, vol. 27, pp. 305–09.
44. R.K.W. Marceau, G. Sha, R.N. Lumley, and S.P. Ringer: *Acta Mater.*, 2010, vol. 58, pp. 1795–1805.
45. R.K.W. Marceau, G. Sha, R. Ferragut, A. Dupasquier, and S.P. Ringer: *Acta Mater.*, 2010, vol. 58, pp. 4923–39.
46. Y. Aruga, D.W. Saxey, E.A. Marquis, A. Cerezo, and G.D.W. Smith: *Ultramicroscopy*, 2011, vol. 11, pp. 725–29.
47. T.H. Courtney: *Mechanical Behavior of Materials*, McGraw-Hill Book Co., Singapore, 2000, pp. 200–02.